Published 03/28/2017

doi:10.4271/2017-01-0133
saealtpow.saejournals.org

Transient Power Optimization of an Organic Rankine Cycle Waste Heat Recovery System for Heavy-Duty Diesel Engine Applications

Bin Xu, Adamu Yebi, Simona Onori, and Zoran Filipi
Clemson-ICAR

Xiaobing Liu, John Shutty, and Paul Anschel
BorgWarner Inc.

Mark Hoffman
Clemson-ICAR

ABSTRACT

This paper presents the transient power optimization of an organic Rankine cycle waste heat recovery (ORC-WHR) system operating on a heavy-duty diesel (HDD). The optimization process is carried on an experimentally validated, physics-based, high fidelity ORC-WHR model, which consists of parallel tail pipe and EGR evaporators, a high pressure working fluid pump, a turbine expander, etc. Three different ORC-WHR mixed vapor temperature (MVT) operational strategies are evaluated to optimize the ORC system net power: (i) constant MVT; (ii) constant superheat temperature; (iii) fuzzy logic superheat temperature based on waste power level. Transient engine conditions are considered in the optimization. Optimization results reveal that adaptation of the vapor temperature setpoint based on evaporation pressure strategy (ii) provides 1.1% mean net power (MNP) improvement relative to a fixed setpoint strategy (i). The highest net power is produced by setpoint strategy (iii), which exhibited a 2.1% improvement compared strategy (i), revealing importance of utilizing engine conditions during reference trajectory generation. These results serve as the benchmark for the ORC system net power optimal control.

CITATION: Xu, B., Yebi, A., Onori, S., Filipi, Z. et al., "Transient Power Optimization of an Organic Rankine Cycle Waste Heat Recovery System for Heavy-Duty Diesel Engine Applications," *SAE Int. J. Alt. Power.* 6(1):2017, doi:10.4271/2017-01-0133.

INTRODUCTION

Recent U.S. regulations on CO_2 emission calls for a 20% reduction in 2020 relative to 2010 [1]. Heavy duty vehicles account for 7% of all on-road vehicles and approximately 30% of the U.S. transportation energy usage [2]. However, over 40% of energy consumed by heavy duty diesel engines (HDD) is wasted as heat [3]. Thus, waste heat recovery (WHR) technologies have been an active area of recent research [4, 5, 6, 7, 8, 9, 10, 11]. There are three main methodologies for vehicle WHR: thermoelectrics, turbo-compounding, and implementation of an organic Rankine cycle (ORC) system.

Thermoelectric strategies generate electricity utilizing the temperature difference between the exhaust gas and the thermoelectric material coolant stream [9, 12, 13]. These devices are compact and simple in structure, but their efficiency is limited by the low ZT value of current thermoelectric materials.

Turbocompounding either combines the turbocharger with an electric generator or couples the device to the engine crankshaft [10, 11, 14]. Turbocompounding recovers kinetic energy from the exhaust gas, which amounts to only a fraction of the total waste heat energy. Much of the waste heat thermal energy still passes to ambient via the exhaust. In addition, turbocompounding generally doesn't consider the waste heat contained in the exhaust gas recirculation (EGR) flow, which comprises nearly 1/3 of the total waste heat in the HDD engine depending on engine operating conditions [15].

An ORC system is able to directly extract thermal energy from tail pipe exhaust gas, EGR, charge air, and even the water jacket [16, 17]. Thus, ORC is the WHR technology with the highest ceiling for recovery heat energy from the multiple streams present on a HDD engine. Literature on ORC-WHR can be divided into two groups: experimental studies and modeling/control studies.

Experimental ORC Studies

Cummins conducted a series of ORC-WHR HDD experiments [18, 19, 20, 21] with funding from U.S. Department of Energy. R245fa was selected as working fluid and a turbine was chosen as the expansion device. They noted a 10% brake thermal efficiency improvement when both the tail pipe exhaust gas and EGR streams were utilized as heat sources [21]. AVL also extensively investigated ORC-WHR research on HDD engine [3, 22, 23, 24, 25, 26, 27]. Ethanol was selected as the working fluid because of its low

evaporation pressure, allowing for lighter and lower cost system components [3]. AVL achieved a 3-5% fuel economy improvement utilizing a turbine as the expansion device. Additionally, Bosch experimentally obtained 2.1kW, 5.3kW and 9.0kW turbine generated power from B25, B50, and B75 engine operating conditions with an ORC system coupled to a 12L HDD engine, respectively [28].

ORC-WHR Modeling and Control

S. Quoilin et al created a finite volume (FV) model of a small-scale R245 ORC-WHR system which utilized a scroll expander [29, 30]. Three control strategies were evaluated for power optimization. The first strategy combined a constant evaporating temperature (via pressure control) and constant superheating temperature for establishing ORC working fluid setpoints. The second strategy utilized an optimal evaporating temperature and constant superheating temperature. In the second case, the optimal evaporating temperature was expressed as a first order polynomial function of working fluid mass flow rate, condensation temperature and heat source inlet temperature through a steady state analysis with Engineering Equation Solver. A third strategy examined optimal working fluid pump speed with a fixed working fluid superheating temperature. Only minimal ORC performance differences were reveled between proposed three control strategies.

Hou et al proposed a power plant scale, 100kW ORC-WHR system model with a turbine expander and R245 as the working fluid [31]. The evaporator was modeled with moving boundary (MB) method. A linear quadratic regulator (LQR) was incorporated with a PI controller to track references of: evaporation pressure, vapor temperature, and power output. The same group proposed a linear model predictive control for the ORC-WHR system and showed a satisfactory working fluid setpoint reference tracking performance over mild transient conditions [32].

Peralez et al presented a model-based control for a steam Rankine cycle waste heat recovery system utilizing a volumetric expander [33]. The evaporator was modeled with the MB method and a reduced order model was derived from the full order MB model. Working fluid superheat temperature and evaporation pressure reference tracking were achieved by a feedback controller and a feedforward controller. The same team proposed transient power optimization for the ORC-WHR via dynamic programming [34]. A 0D heat exchanger model was utilized for computational efficiency, while the engine conditions for the optimization were a mild step-change transient.

Xu et al proposed an ORC-WHR system model for HDD application [4]. The parallel EGR and exhaust tailpipe evaporators were modeled with FV method, a turbine was selected as the expansion device, and ethanol was chosen as working fluid. Steady state turbine power optimization was conducted by analyzing the relationship between the expansion turbine and four actuators: working fluid pump speed, mass flow distribution between the parallel evaporators, turbine speed, and coolant pump speed [15].

Yebi et al proposed a nonlinear model predictive controller operating over parallel MB evaporator models for HDD engine ORC-WHR system extracting heat from both the EGR and tailpipe streams [35]. Comparisons between MPC and PID control over the mixed vapor temperature at the outlet of parallel evaporators showed the merit of MPC utilization during working fluid vapor setpoint changes at constant engine conditions.

Transient ORC-WHR Optimization

Even with the wealth of prior ORC research, transient power optimization for an ORC system operating on a HDD engine is rarely researched. Even though Quoilin et al considered different control strategies to optimize the ORC-WHR system power output, that ORC system was designed for a small scale waste heat source with a low temperature range (120-300°C), which is below the typical temperature of HDD engine exhaust gas and EGR streams (300-500°C) [29]. Meanwhile, the optimal temperature was calculated based on steady state, which does not account for heat exchanger thermal inertia. Additionally, while Peralez et al optimized ORC power with dynamic programming over transient engine conditions, the transient condition was merely a mild step change rather than a transient drive cycle [34]. This paper studies the HDD engine power optimization over highly transient engine conditions with a experimentally validated, physics-based, high fidelity ORC-WHR model [4].

Working fluid saturation temperature is the optimal vapor temperature reference with respect to maximizing turbine generated power. However, if saturation temperature is utilized as the control reference, then the ORC system controller must perfectly maintain the exact saturation temperature or risk harming the turbine expander via exposure to working fluid with vapor quality below unity. Therefore, for imperfect controllers, the working fluid temperature reference trajectory must be set greater than the saturation temperature. The greater the working fluid temperature oscillation allowed by the controller, the larger this buffer in control reference temperature must be.

In this work, three ORC working fluid vapor temperature reference creation strategies are described and evaluated over a HDD highly transient driving cycle. The strategies focus on control of the mixed working fluid vapor temperature (i.e. the pre-turbine condition where which combines the outlets of the parallel EGR and tailpipe evaporators). The pre-turbine mixed working fluid reference setpoint strategies addressed herein are: (i) constant working fluid vapor temperature (ii) constant working fluid superheat temperature, and (iii) a fuzzy logic working fluid vapor temperature.

This paper is organized as follows: The ORC-WHR system configuration overview is described and then the component modeling section follows to give a brief introduction of the FV model. After that, the transient optimization problem is formulated and optimization results are analyzed. Lastly, the paper ends with discussion and conclusions.

EXPERIMENTAL ORC-WHR SYSTEM CONFIGURATION

Modern diesel engines typically operate with high pressure exhaust gas recirculation (EGR), making the EGR stream an attractive heat source for a diesel WHR system. The inclusion of EGR as a heat source (along with the exhaust flow) creates options for the connection of the two heat exchangers: in series or in parallel. The parallel configuration is suitable for high mass flow with less pressure loss because the cross sectional area of working fluid flow path increases. A series evaporator connection produces higher working fluid vapor temperatures because the long flow path aides superheat. Considering higher mass flow has been proven fortuitous for power generation [5], the parallel configuration was chosen, and is shown in Figure 1.

The ORC system components are connected in a standard ORC loop, specifically: (i) a low pressure working fluid supply pump , (ii) a high pressure working fluid pump, (iii) two mass flow valves which distribute the working fluid between the evaporators, (iv) two parallel evaporators, (v) an exhaust bypass valve, (vi) a valve upstream of the turbine expander, (vii) a valve before the turbine to bypass liquid working fluid when the system is in warm-up or cool-down state, (viii) a turbine expander for electricity generation, (ix) a condenser downstream of the turbine, and (x) an expansion tank between condenser and low pressure pump to buffer the working fluid flow. This system utilizes ethanol as the working fluid.

A 13L heavy duty diesel engine is connected with the ORC-WHR system. The only connections between engine and ORC-WHR system are the tail pipe (TP) and EGR evaporators, shown in Figure 1. During normal operating conditions, exhaust gas flows through the TP evaporator and transfers heat to the working fluid. A TP evaporator bypass valve is installed to protect the ORC-WHR working fluid from overheat and subsequent working fluid degradation when engine operates at high load. The EGR evaporator replaces the stock EGR intercooler. Due to EGR evaporator outlet temperature constraints, there is no bypass valve installed in the EGR line. The working fluid mass flow to the parallel evaporators is controlled by valves located between the high pressure pump and their respective evaporator.

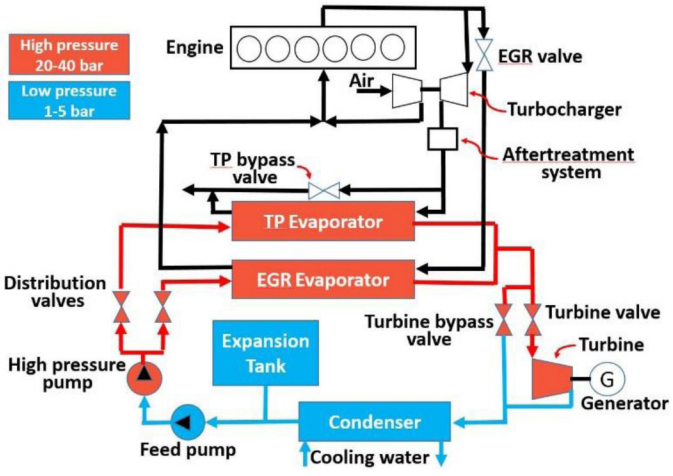

Figure 1. Schematic of ORC-WHR system

ORC COMPONENT MODEL DESCRIPTIONS

The ORC-WHR system is simulated with a physics-based high fidelity model for this transient evaluation. A complete description of the model and its governing equations can be found in [4]. However, the following is a basic summary of the model's principles.

The evaporators are modeled with the FV method, which discretizes the working fluid flow volume, exhaust flow volume and wall volume into 30 cells. Mass balance, energy balance and momentum balance equations are solved in each cell. Working fluid phase boundaries can be interpolated by the vapor quality of each cell. Meanwhile, the high pressure pump supplying working fluid to the evaporators is a positive displacement type and the mass flow rate varies linearly with pump revolution speed.

There are five valves in the system. The two mass flow distribution valves located before the parallel evaporators are modeled as control valves with exposure to incompressible liquid because these two valves control pure liquid ethanol at all times. Another control valve, located before the turbine expander, is modeled as controlling compressible vapor since it opens only when the vapor quality is sufficiently high to protect the turbine from damage. The control valve parallel to the turbine expander interacts with both incompressible liquid and compressible vapor working fluid as the system warms, and is modeled accordingly. The TP bypass valve is modeled as simple on/off binary valve and pressure drop is not considered in the open position. Again, complete modeling details of each component within the ORC system can be found in [4]. However, some updates have been made, namely:

The turbine expander model has been updated since the referenced work was published and now takes the form:

$$P_{turb} = \eta_{thermal}\dot{m}_{turb}\left(h_{turb,in} - h_{turb,out,is}\right) \quad (1)$$

where P_{turb} is turbine generated power , $\dot{m}_{turb}$ is turbine mass flow rate, $h_{turb,in}$ is turbine inlet enthalpy, and $h_{turb,out,is}$ is turbine outlet isentropic enthalpy. Thermal efficiency $\eta_{thermal}$ is interpolated from a turbine map which contains the functional dependences shown in (Eq. 2)

$$\eta_{thermal} = map(N_{turb}, p_{in}, p_{out}) \quad (2)$$

where N_{turb} is turbine speed, P_{in},p_{out} are turbine inlet and outlet pressure. The operating expansion ratio for the turbine expander ranges from 5-30, which is relatively high compared to typical turbo-charger [36, 37]. The high expansion ratio leads to choked flow of the turbine and thus the mass flow rate has linear relationship with the inlet pressure:

$$\dot{m}_{turb} = a_{turb,1}p_{in} + a_{turb,2} \quad (3)$$

where $a_{turb,1}$ and $a_{turb,2}$ are two constant coefficients. Turbine outlet enthalpy is calculated as follows:

$$h_{turb,out} = h_{turb,in} - \eta_{thermal}(h_{turb,in} - h_{turb,out,is}) \quad (4)$$

$$h_{turb,out,is} = map(s_{turb,out}, p_{out}) \quad (5)$$

$$s_{turb,out} = s_{turb,in} \quad (6)$$

$$s_{turb,in} = map(h_{turb,in}, p_{in}) \quad (7)$$

where $s_{turb,in}$, $s_{turb,out}$ are inlet and outlet entropy.

OPTIMIZATION PROBLEM FORMULATION

The goal of the optimization problem is to maximize the net power from the ORC-WHR system. Assumptions made for the optimization are: (i) condenser power consumption is not considered and outlet temperature is constant; (ii) valve actuation power consumption is not considered; and (iv) power consumed by the low pressure feed pump is negligible. With those assumptions, the net power is defined as follows:

$$P_{net} = P_{turb} - P_{HPP} \quad (8)$$

The system actuators are described as follows: (i) A high pressure pump controls the mixed vapor temperature after the parallel evaporators via both a feedforward control and PID feedback control. The feedforward control is based on the total waste heat power in tail pipe exhaust gas and EGR exhaust gas. (ii) Two mass flow distribution valves control the temperature difference of the ethanol vapor between the parallel evaporator outlets. Mass flow distribution is controlled with a feedforward plus PID feedback. The feedforward control is based on the ratio of waste heat power between tail pipe exhaust gas and EGR exhaust gas. (iii) The turbine bypass valve can be utilized to control the evaporation pressure, and its controller is also feedforward plus PID feedback control. The feedforward control is based on the measured high pressure pump speed, measured pre-turbine working fluid temperature, pre-turbine pressure setpoint, and measured turbine speed. The gains of the controllers are all calibrated on the experimental test rig. (iv) The condenser coolant pump speed is closed loop controlled so that the ethanol at the condenser outlet maintains a pure liquid state. (v) Turbine speed is real-time optimized for maximum efficiency based on the inlet and outlet pressure and the turbine thermal efficiency map (Eq. 2). The optimal speed for maximum efficiency is found for each pair of inlet and outlet pressure as follows:

$$N^*_{turb} = arg\max_{N_{turb}}[map(N_{turb}, p_{in}, p_{out})] \quad (9)$$

The working fluid distribution values (actuator ii) are controlled to maintain the difference between the two evaporator outlet temperatures at zero. Meanwhile, the turbine bypass valve (actuator iii) is used for pressure relief when the evaporation pressure exceeds 35 bar, the condenser coolant pump speed (actuator iv) is utilized to maintain 30 °C working fluid at the condenser outlet. Turbine speed (actuator v) is real-time optimized for maximum efficiency. Therefore, only the high pressure pump speed (actuator i) is left to optimize the pre-turbine mixed vapor temperature.

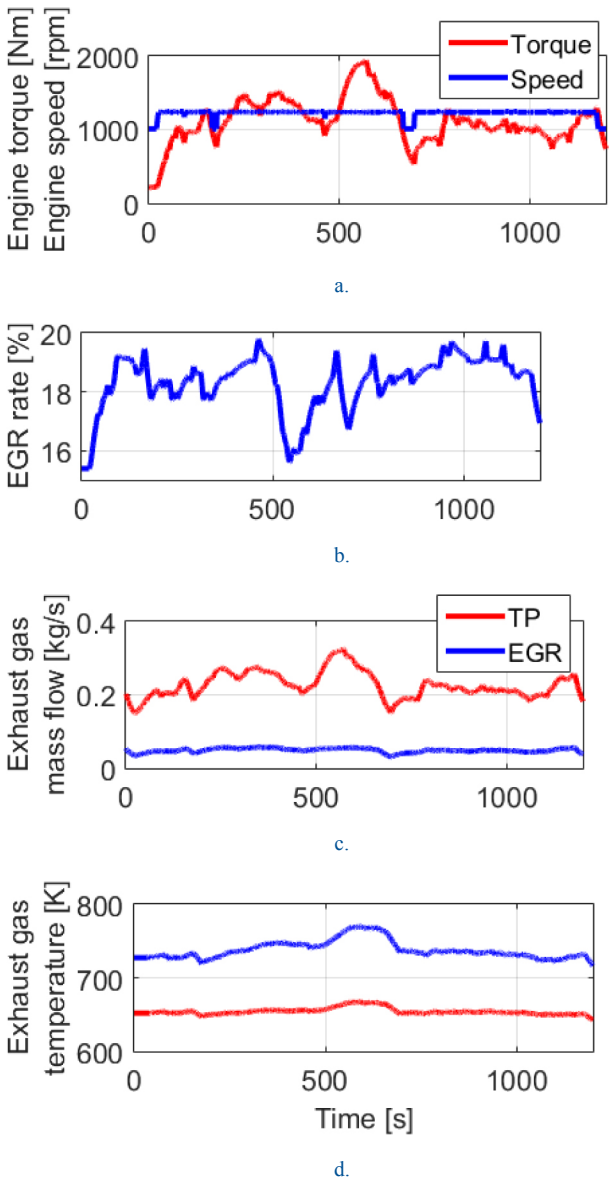

Figure 2. (a) Engine speed and toque, (b) EGR rate, (c) Tail pipe exhaust gas and EGR mass flow rate at the inlet of evaporators and (d) Tail pipe and EGR temperature at the inlet of evaporators.

The transient engine conditions considered for the optimization comprise a constant speed, variable load transient cycle. Figure 3 depicts the time varying engine speed/torque (Figure 2a) and EGR rate (Figure 2b) profiles. While speed is nearly constant, the torque is highly transient, representing a typical HDD duty cycle for long haul applications. The EGR and TP exhaust gas mass flow rates and temperatures are obtained from a GT-POWER engine model simulation, and the results are shown in Figure 2c and 2d, respectively.

Three pre-turbine mixed vapor temperature (MVT) reference strategies are compared in this paper: (i) constant MVT; (ii) constant superheat temperature; (iii) fuzzy logic superheat temperature based on waste heat power level. For strategy (i), MVT is swept between 200°C to 320°C in 10°C increments:

$$MVT_1 = const\ (const \in [200,320]) \tag{10}$$

In strategy (ii), the working fluid superheat quantity is swept between 10°C and 100°C in 10°C increments. During the simulation, saturation temperature is time dependent, making the MVT of strategy (ii) time dependent as well. As calculated MVT summed with the desired superheat quantity may exceed ethanol decomposition temperature, operation is capped at 320°C.

$$MVT_2 = \begin{cases} const + T_{sat}, & MVT_2 \le 320^oC \\ 320, & MVT_2 > 320^oC \end{cases} \quad (const \in [10,100]) \tag{11}$$

For the fuzzy logic strategy (iii), MVT is set as follows:

$$MVT_3 = \begin{cases} const_1 + T_{sat}, \ P_{max,exh} \ge P_{exh} \ge P_1 \\ \vdots \\ const_n + T_{sat}, \ P_{n-1} \ge P_{exh} \ge P_{min,exh} \end{cases}$$

$$const_j \in [10,120]\ (j = 1,2,\dots,n) \tag{12}$$

where $const_j$ is j^{th} superheat reference based on engine waste power level, $P_{min,exh}$ *and* $P_{max,exh}$ are minimum and maximum waste heat power over the transient cycle, and exhaust waste power P_{exh} is given below:

$$P_{exh} = \dot{m}_{TP} C_{p,TP} (T_{TP} - T_{amb}) + \dot{m}_{EGR} C_{p,EGR} (T_{EGR} - T_{amb}) \tag{13}$$

where $\dot{m}_{TP}$, $\dot{m}_{EGR}$ are tailpipe and EGR mass flow rates, $C_{p,TP}$ and $C_{p,EGR}$ are tailpipe and EGR exhaust gas heat capacities, respectively, T_{TP} and T_{EGR} are tailpipe and EGR temperature, respectively, and T_{amb} is ambient temperature.

Three parameters need to be optimized for the fuzzy logic control strategy (iii): the number of piecewise control references desired (n), the number of discrete waste heat power levels to consider P_i (i=1,2,…,n-1), and the desired level of superheat in each chosen waste heat power region $const_j$ (j=1,2,…,n). Considering the computation cost, n is selected as 2 for this paper. Thus, two constant superheat references are defined for the lower and higher engine waste heat conditions. Because the engine conditions are highly transient, the switching frequency between the two superheat references is very high, which increases the burden of the controller and may cause vapor temperature oscillations. To overcome this issue, a low pass filter is applied to the MVT reference. The expression for the low pass filter is given in Eqs. 14 and 15. The filtered MVT reference results along the cycle are shown in Figure 3.

$$MVT_{filter}(k) = \frac{0.5}{1000.5} * [C * const_1 + C * const_2] + \frac{1000}{1000.5} MVT_{filter}(k-1) \tag{14}$$

$$C = \begin{cases} 0, if\ P_{max,exh} \ge P_{exh} \ge P_1 \\ 1, if\ P_1 > P_{exh} \ge P_{min,exh} \end{cases} \tag{15}$$

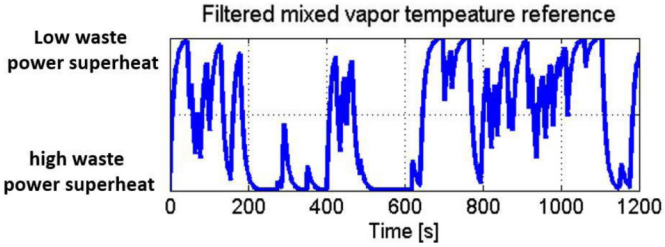

Figure 3. Strategy (iii) reference shape along the cycle

OPTIMIZATION RESULTS

Strategy (i) – Constant MVT Reference

The results from the constant mixed vapor temperature reference selection strategy are shown in Figure 4. Only three typical references are displayed for visibility. Accumulated energy, net power and mixed vapor temperature are normalized by their maximum value. The accumulated energy is calculated as follows:

$$E_{ac} = \sum_{i=1}^{T_{sim}/\Delta t} [P_{net}(i)\Delta t] \tag{16}$$

where T_{sim} is total cycle simulation time, Δt is simulation time step, and $P_{net}(i)$ is the net power produced at i^{th} time step.

The accumulated energy indicates that that accumulated energy increases as the constant MVT reference is reduced. In Figure 4b, the net power profile across the cycle shares a similar shape with exhaust gas mass flow rates. Figure 4c illustrates the MVT control difficulty for highly transient engine condition. The MVT control performance difference is negligible at the setpoints.

The accumulated energy is calculated by integrating the net power along the time series for each reference case and it is plotted in Figure 5 (left y axis). Meanwhile, the turbine operational duration, expressed as a percentage of total cycle time is shown on the right y axis. The accumulated power increases as the MVT reference decreases from the maximum boundary and peaks when MVT is equal to 230°C, the lowest possible setpoint before the turbine operational duration begins to decrease. Subsequent reduction of MVT results in a continued decrease of turbine operational duration and a decrease in accumulated energy.

The cumulative duration of turbine operation helps explain the accumulated energy trend as follows: as MVT is increased, turbine operational duration increases since the controller produces fewer excursions out of the superheated working fluid phase, which increases total power generation time and thus the accumulated

energy. When MVT is above 230°C, the turbine is capable of operation throughout the entire transient cycle. During this period, the working fluid mass flow rate is the most important parameter affecting the power generation rather than turbine operation time. As MVT continues to increase, the working fluid mass flow rate decreases and turbine generated power decreases. Even though less working fluid mass flow rate requires less pump power consumption, this power consumption reduction is negligible compared with the turbine power decrease. For the working fluid influence on turbine power generation, refer to [15].

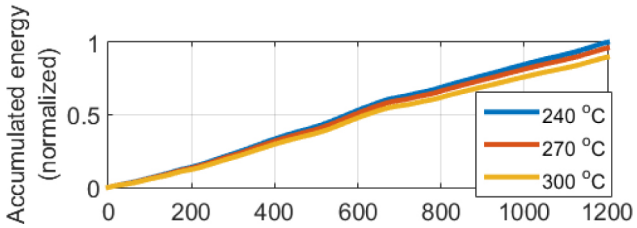

a.

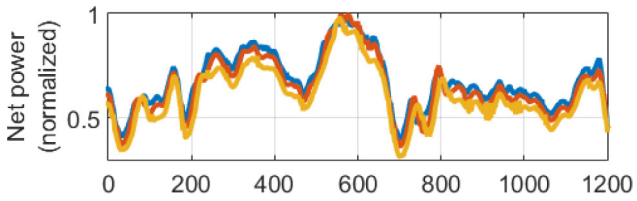

b.

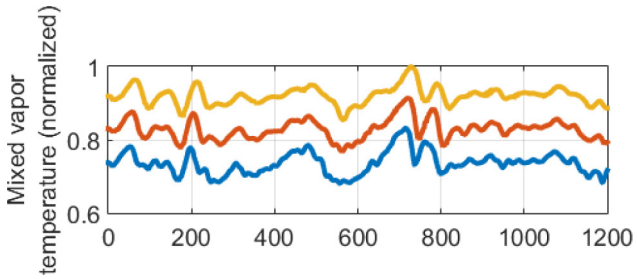

c.

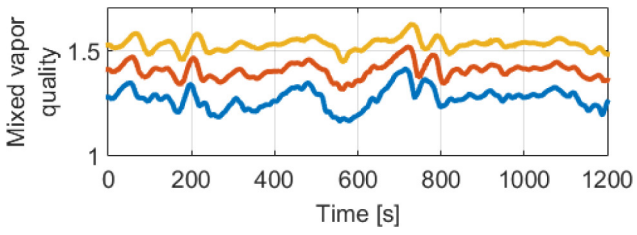

d.

Figure 4. (a) Accumulated energy, (b) net power output,(c) mixed vapor temperature and (d) mixed vapor quality results from strategy (i) (three mixed vapor temperature references: 240°C, 270°C, and 300°C)

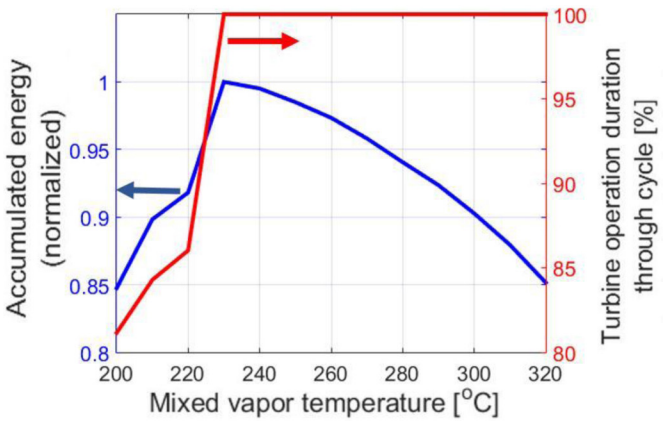

Figure 5. Accumulated energy and turbine operation duration percentage through the whole cycle from the constant MVT reference strategy

Strategy (ii) – Constant Superheat MVT

The optimization results from strategy (ii) are shown in Figure 6. The net power, MVT and mixed vapor quality share similar profiles to those resulting from the "constant MVT reference strategy (i)" shown in Figure 4.

Accumulated energy for strategy (ii) is normalized based on its maximum accumulated energy and is shown in Figure 7 along with turbine operation duration percentage. Overall, strategy (ii) generates 1.1% more power than strategy (i). The explanation for the shape of the accumulated energy trend is similar to that of strategy (i): with less than 50°C superheat, net power is mainly affected by turbine operation duration, which is influenced by mixed phase working fluid produced in the low superheat reference conditions. With greater than 50°C, superheat, turbine operation duration percentage is nearly constant at 100% and net power is mainly affected by working fluid mass flow rate. During highly transient engine condition, working fluid mass flow rate follows waste heat power profiles. Compared with exhaust gas temperature, exhaust gas mass flow rate change is more significant in Figure 2. Thus, working fluid mass flow rate profile share the similar profile with exhaust gas mass flow rates.

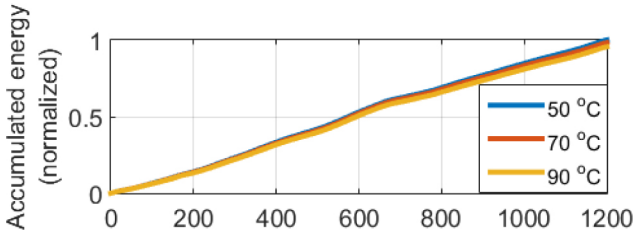

a.

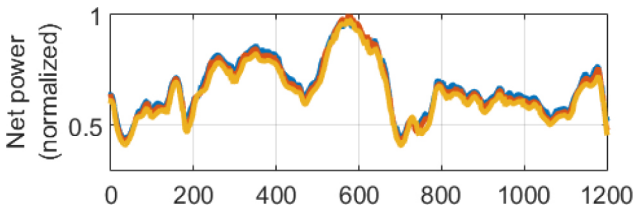

b.

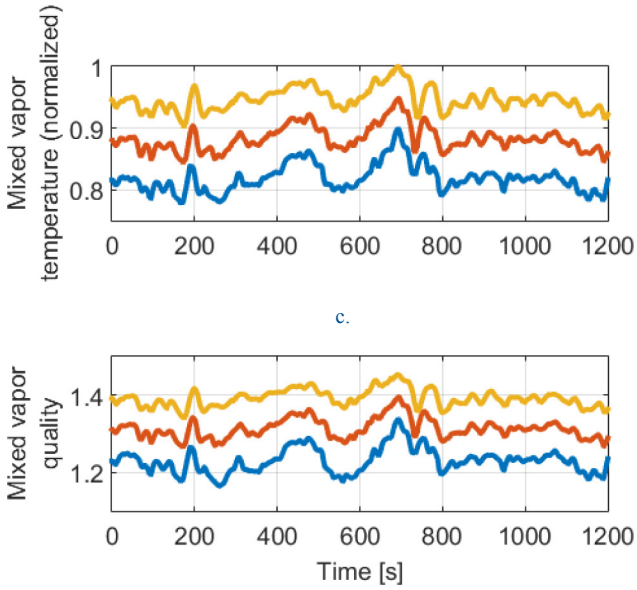

Figure 6. (a) Accumulated energy, (b) net power output, (c) mixed vapor temperature and (d) mixed vapor quality results from strategy (ii): fixed quantity of superheat (three superheat temperature references are shown: 50°C, 70°C , and 90°C)

The constant superheat MVT reference strategy (ii) has another advantage over constant MVT reference strategy (i) during the highly transient engine condition, which is explained by the time-variant MVT of the constant superheat reference generation (strategy ii). For example, if strategy (i) sets a constant MVT reference at 200°C, this temperature is below the saturation temperature if evaporation pressure rises above 30bar during a transient. At that time, the mixed vapor quality will fall below 1.05 and the turbine inlet valve closes to protect the turbine, halting the generation of power. However, strategy (ii) improves this situation by adapting the MVT based on saturation temperature and maintaining a fixed superheat temperature above saturation. However, the reason for the decay in accumulated energy at low superheat values is due to controller oscillations, which allow MVT excursions below the saturation dome.

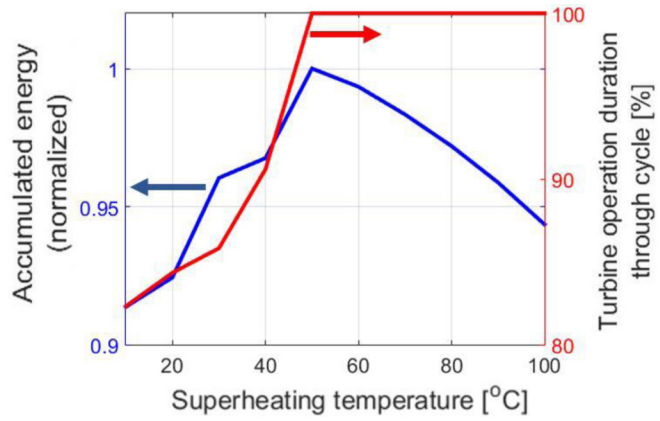

Figure 7. Accumulated energy and turbine operation duration percentage through the whole cycle from constant superheat MVT strategy

Strategy (iii) Fuzzy Logic Mixed Vapor Temperature Setpoint

The accumulated ORC energy for the fuzzy logic MVT reference strategy (iii) is shown in Figure 8. The peak of this accumulated energy dome is not in the center of the chosen ranges for low and high waste power superheat, which is not surprising as the differing exhaust power levels chosen may produce the maximum ORC power with different superheat references. When this system and controller operates at 'low waste power superheat', it performs more optimally with a modest superheat target. Maximum accumulated energy over the transient engine conditions occurs when the superheat reference is set between 40-80°C for high waste heat power levels while the reference for operation during lower waste power superheat is simultaneously chosen between 50-70°C superheat. It should be noted that the disparity between the superheat setpoints also holds influence over the simulation results of strategy (iii) via the reference switching trajectory of Figure 3. Large disparities between absolute working fluid setpoints may result in controller overshoot, which can degrade the total turbine power generation time.

Throughout the ranges of setpoints, accumulated ORC energy is more sensitive to the high waste power superheat value than the low waste power superheat value. Variation of high waste power superheat specification given a fixed low waste power superheat constant leads to more than a 10% change in accumulated ORC energy. Whereas, given a fixed high waste power superheat value, variation of low waste power superheat reference produces only a 6% change in accumulated energy. However, the relative sensitivity of ORC power to the high and low power constants depends on both the power thresholds utilized by the fuzzy logic piece-wise implementation and how those thresholds interplay with the particular drive cycle.

Overall, in the chosen power split configuration, the high waste power superheat reference value has more influence on accumulated energy over the transient engine conditions than low waste power superheat reference. The fuzzy logic superheat reference strategy (iii) produces 2% more accumulated ORC energy than the fixed mixed vapor temperature strategy (i) as shown in Figure 10.

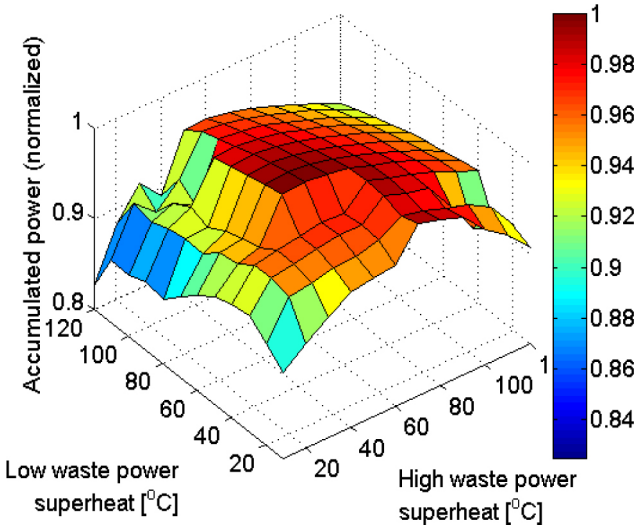

Figure 8. Normalized accumulated power for the fuzzy logic MVT reference strategy

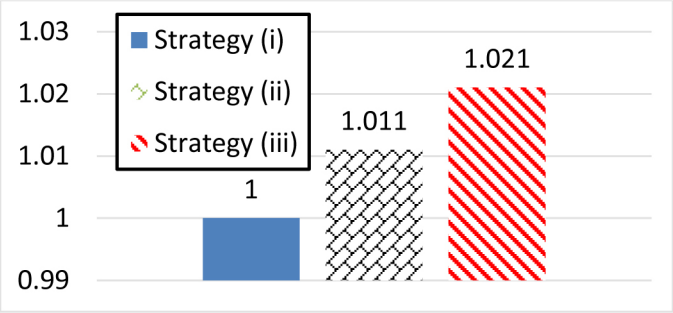

Figure 10. Mmaximum accumulated energy comparison for the three MVT reference strategies. Strategy (i) is selected as baseline reference, based on which, strategies (ii) and (iii) increased accumulated energy by 1.1% and 2.1% respectively.

DISCUSSION

The fixed mixed vapor temperature ORC reference strategy (i) and constant superheat reference strategy (ii) present slightly inferior performance compared with fuzzy logic switching between multiple superheat references, strategy (iii). The absolute performance of all three strategies is influenced by the MVT controller response and its ability to maintain the desired vapor temperature reference over these highly transient engine conditions, which is a challenging task. With a more precise MVT controller, the MVT reference can be further reduced without the ORC system experiencing MVT excursions within the vapor dome, avoiding shutdown of the turbine expander and elongating the turbine power production duration. Meanwhile, reduced actuation of turbine valve is beneficial for component life. Moreover, increasing the MVT controller precision will prevent ethanol decomposition by limiting MVT excursions beyond the decomposition limits.

There is still room to improve the fuzzy logic strategy (iii). In this paper, due to computation cost, only two regions for the exhaust waste heat power discretization are considered. If the number of discrete superheat reference regions is increased, the MVT reference flexibility to the exhaust waste heat power will increase as well. Generally, the optimal performance for strategy (iii) can be achieved when the number of piece-wise regions approaches infinity. Furthermore, a higher resolution of high waste power superheat discretization or utilization of optimization algorithms (e.g. Particle Swarm Optimization [38], Genetic Algorithm [39], etc.) may identify a ”more optimal” superheat reference value in each discrete power region. Meanwhile, bear in mind that the power threshold for the fuzzy logic of strategy (iii) was not optimized for the operational cycle. Thus, the differences among the three strategies needs further investigation.

CONCLUSIONS

Transient power optimization of ORC-WHR system is carried out over transient engine conditions with a validated, high fidelity, physics-based model. Reference values for the pre-turbine mixed working fluid vapor temperature are selected based on three strategies: (i) constant MVT; (ii) constant superheat temperature; (iii) fuzzy logic superheat temperature based on waste power level. Optimized accumulated ORC energy from strategy (i) is within 1.1% of strategy (ii) over transient engine conditions. The advantage of strategy (ii) relative to strategy (i) is created by implementation of an adaptive MVT reference temperature. This adaptive reference generation reduces the burden on the PID controller and thus improves the controller robustness and system performance during the highly transient engine conditions. The fuzzy logic strategy (iii) shows 2.1% net power increase compared with strategy (i) by implementing adaptation saturation temperature references which are sensitive to waste heat power.

The authors believe there is still room to improve the fuzzy logic transient power optimization strategy (iii). Parameters like the number of different waste heat power regions and the waste power boundary locations can be optimized to further improve the accumulated power. Moreover, increasing the precision of the MVT controller will bolster accumulated energy for all strategies over highly transient engine conditions. Finally, adding condenser power consumption and valve actuation power consumption into the net power expression will be more realistic.

Moving forward, the optimization results from this paper will be compared with the transient power optimization results of a model predictive controller, which was developed in [35]. Meanwhile, experiments will be conducted to validate the optimization results.

REFERENCES

1. EPA, “EPA and NHTSA adopt first-ever program to reduce greenhouse gas emissions and improve fuel efficiency of medium- and heavy-duty vehicles,” 2011.
2. ICCT, “United States Efficiency and greenhouse Gas Emission Regulations for Model Yeat 2018-2027 Heavy-Duty Vehicles, Engines and trailers,” 2015.
3. Park, T. Teng, H. Hunter, G. L. van der Velde, and B. Klaver, J. “A Rankine Cycle System for Recovering Waste Heat from HD Diesel Engines - Experimental Results,” SAE International, Warrendale, PA 2011-01-1337, 2011/04// 2011.
4. Xu, B. Liu, X. Shutty, J. Anschel, P. Onori, S. Filipi, Z. , “Physics-Based Modeling and Transient Validation of an Organic Rankine Cycle Waste Heat Recovery System for a Heavy-Duty Diesel Engine,” SAE Technical Paper 0148-7191, 2016.
5. Feru, E. Willems, F. de Jager, and B. Steinbuch, M. “Modeling and Control of a Parallel Waste Heat Recovery System for Euro-VI Heavy-Duty Diesel Engines,” *Energies*, vol. 7, pp. 6571–6592, 2014/10/14/ 2014.
6. Horst, T. A. Rottengruber, H.-S. Seifert, and M. Ringler, J. “Dynamic heat exchanger model for performance prediction and control system design of automotive waste heat recovery systems,” *Applied Energy*, vol. 105, pp. 293–303, 2013/05// 2013.
7. Yamamoto, T. Furuhata, T. Arai, and N. Mori, K. “Design and testing of the Organic Rankine Cycle,” *Energy*, vol. 26, pp. 239–251, Mar 2001.
8. Liu and C. Zhong Li W., “An Experimental Study of a Novel Prototype for Thermoelectric Power Generation from Vehicle Exhaust,” *Distributed Generation & Alternative Energy Journal*, vol. 28, pp. 32–48, 2013 2013.
9. Zhou Minfeng H. Y. a. C. Y., “Numerical Simulation of the Thermoelectric Model on Vehicle Turbocharged Diesel Engine Intercooler,” *Research Journal of Applied Sciences, Engineering and Technology*, p. 5, 2014/08/02/18:27:12 2013.
10. Edwards, K., Wagner, R., and Briggs, T., “Investigating Potential Light-duty Efficiency Improvements through Simulation of Turbo-compounding and Waste-heat Recovery Systems,” SAE Technical Paper 2010-01-2209, 2010, doi:10.4271/2010-01-2209.
11. Ismail, Y., Durrieu, D., Menegazzi, P., Chesse, P. , “Potential of Exhaust Heat Recovery by Turbocompounding,” SAE Technical Paper 2012-01-1603, 2012, doi:10.4271/2012-01-1603.
12. Crane, D., Jackson, G., and Holloway, D., “Towards Optimization of Automotive Waste Heat Recovery Using Thermoelectrics,” SAE Technical Paper 2001-01-1021, 2001, doi:10.4271/2001-01-1021.

13. Hendricks and T. J. Lustbader, J. A. "Advanced thermoelectric power system investigations for light-duty and heavy duty applications. I," in *Twenty-First International Conference on Thermoelectrics, 2002. Proceedings ICT '02*, 2002, pp. 381–386.
14. Hountalas, D., Katsanos, C., and Lamaris, V., "Recovering Energy from the Diesel Engine Exhaust Using Mechanical and Electrical Turbocompounding," SAE Technical Paper 2007-01-1563, 2007, doi:10.4271/2007-01-1563.
15. Xu, B. Yebi, A. Onori, S. Filipi, Z. Liu, X. Shutty, J. , "Power Maximization of a Heavy Duty Diesel Organic Rankine Cycle Waste HEat Recovery System Utilizing Mechanically Coupled and Fully Electrified Turbine Expanders," in Proceedings of the ASME 2016 Internal Combustion Fall Technical Conference, Greenville, SC, USA,2016, p. 11.
16. Arias, D., Shedd, T., and Jester, R., "Theoretical Analysis of Waste Heat Recovery from an Internal Combustion Engine in a Hybrid Vehicle," SAE Technical Paper 2006-01-1605, 2006, doi:10.4271/2006-01-1605.
17. Delgado and O. Lutsey, N. "The U.S SuperTruck Program: Expediting the Development of Advanced Heavy-Duty Vehicle Efficiency Technologies," The International Council on Clean Transportation2014.
18. Nelson, C. R. "Exhaust Energy Recovery," presented at the Presentation at USDOE Directions in Engine-Efficiency and Emissions Research Conference, 2006.
19. Nelson, C. R. "Exhaust Energy Recovery," presented at the Presentation at USDOE Directions in Engine-Efficiency and Emissions Research Conference, 2008.
20. Nelson, C. R. "Exhaust Energy Recovery," presented at the Presentation at USDOE Directions in Engine-Efficiency and Emissions Research Conference, 2009.
21. Nelson, C. R. "Exhaust Energy Recovery," presented at the Presentation at USDOE Directions in Engine-Efficiency and Emissions Research Conference, 2010.
22. Teng, H., "Waste Heat Recovery Concept to Reduce Fuel Consumption and Heat Rejection from a Diesel Engine," *SAE Int. J. Commer. Veh.*3(1):60–68, 2010, doi:10.4271/2010-01-1928.
23. Teng, H., Klaver, J., Park, T., Hunter, G. , "A Rankine Cycle System for Recovering Waste Heat from HD Diesel Engines - WHR System Development," SAE Technical Paper 2011-01-0311, 2011, doi:10.4271/2011-01-0311.
24. Teng, H. and Regner, G., "Improving Fuel Economy for HD Diesel Engines with WHR Rankine Cycle Driven by EGR Cooler Heat Rejection," SAE Technical Paper 2009-01-2913, 2009, doi:10.4271/2009-01-2913.
25. Teng, H., Regner, G., and Cowland, C., "Achieving High Engine Efficiency for Heavy-Duty Diesel Engines by Waste Heat Recovery Using Supercritical Organic-Fluid Rankine Cycle," SAE Technical Paper 2006-01-3522, 2006, doi:10.4271/2006-01-3522.
26. Teng, H., Regner, G., and Cowland, C., "Waste Heat Recovery of Heavy-Duty Diesel Engines by Organic Rankine Cycle Part I: Hybrid Energy System of Diesel and Rankine Engines," SAE Technical Paper 2007-01-0537, 2007, doi:10.4271/2007-01-0537.
27. Teng, H., Regner, G., and Cowland, C., "Waste Heat Recovery of Heavy-Duty Diesel Engines by Organic Rankine Cycle Part II: Working Fluids for WHR-ORC," SAE Technical Paper 2007-01-0543, 2007, doi:10.4271/2007-01-0543.
28. Seher, D. Lengenfelder, T. Jurgen, G. Nadja, E. Michael, and H. Krinn, I. "Waste Heat Recovery for Commercial Vehicles with a Rankine Process," *21st Aachen Colloquium Automobile and Engine technology*, 2012.
29. Quoilin, S. Lemort, and V. Lebrun, J. "Experimental study and modeling of an Organic Rankine Cycle using scroll expander," *Applied Energy*, vol. 87, pp. 1260–1268, Apr 2010.
30. Quoilin, S. Aumann, R. Grill, A. Schuster, A. Lemort, and V. Spliethoff, H. "Dynamic modeling and optimal control strategy of waste heat recovery Organic Rankine Cycles," *Applied Energy*, vol. 88, pp. 2183–2190, 6// 2011.
31. Zhang, J. H. Zhang, W. F. Hou, and G. L. Fang, F. "Dynamic modeling and multivariable control of organic Rankine cycles in waste heat utilizing processes," *Computers & Mathematics with Applications*, vol. 64, pp. 908–921, Sep 2012.
32. Zhang, J. H. Zhou, Y. L. Li, Y. Hou, and G. L. Fang, F. "Generalized predictive control applied in waste heat recovery power plants," *Applied Energy*, vol. 102, pp. 320–326, Feb 2013.
33. Peralez, J. Tona, P. Sciarretta, A. Dufour, and P. Nadri, M. "Towards model-based control of a steam Rankine process for engine waste heat recovery," *2012 Ieee Vehicle Power and Propulsion Conference (Vppc)*, pp. 289–294, 2012.
34. Peralez, J. Tona, P. Sciarretta, A. Dufour, and P. Nadri, M. "Optimal control of a vehicular organic rankine cycle via dynamic programming with adaptive discretization grid," *IFAC Proceedings Volumes*, vol. 47, pp. 5671–5678, 2014.
35. Yebi, A. Xu, B. Liu, X. Shutty, J. Anschel, P. Onori, S. , "Nonlinear Model Predictive Control of a Parallel Evaporator Waste Heat Recovery System for Heavy-Duty Diesel Engines Applications," in Proceedings of ASME Dynamic System and Control Conference, Minneapolis, Minnesota, USA, 2016.
36. Nasser, S. and Playfoot, B., "A Turbocharger Selection Computer Model," SAE Technical Paper 1999-01-0559, 1999, doi:10.4271/1999-01-0559.
37. Sun, H., Hanna, D., Niessen, P., Fulton, B. , "Experimental Evaluation of Advanced Turbocharger Performance on a Light Duty Diesel Engine," *SAE Int. J. Engines*6(2):788–796, 2013, doi:10.4271/2013-01-0920.
38. Ebbesen, S. Kiwitz, and P. Guzzella, L. "A Generic Particle Swarm Optimization Matlab Function," *2012 American Control Conference (Acc)*, pp. 1519–1524, 2012.
39. Deb, K. Pratap, A. Agarwal, and S. Meyarivan, T. "A fast and elitist multiobjective genetic algorithm: NSGA-II," *Ieee Transactions on Evolutionary Computation*, vol. 6, pp. 182–197, Apr 2002.